1

Formation Testing – Background, Perspectives and New Industry Requirements

Oil and gas industry petrophysicists are well versed in well logging methodologies. And over the past several decades, a large suite of formation evaluation instruments have seen commercial introduction, tools measuring, for example, resistivity, sonic speed, gamma ray, nuclear magnetic resonance properties, and so on. We *know* what they measure, or at least, think we do. Take resistivity analysis. We intuitively conjure up images related to DC resistance, a property often highlighted by the differences in intensity associated with dim versus bright light bulbs. But the interpretation of measured quantities in reality depends on subtleties beyond the experience of even experienced analysts. For instance, one might ask, "How does invasion affect measurements and how are these corrected?" "Were predictions derived from phase or amplitude data?" Or, "How extensive was the simulation domain used to derive interpretation charts and what is its influence?"

1.1 Formation Testing – A Brief Introduction.

The point is, for just about all logging tools, analogous subtleties arise that are not easily addressed – measured data in all cases are *indirect* and subject to cross-checks between different tools, plus (hopeful) familiarity with the geological asset. When one of the authors asked Rob Kirby, an experienced directional driller in Houston, "Which logging measurement would *you* prefer, given all that are commercially available?" His response was, "I'd take formation testing any day." And the reason? It was obvious. The formation tester provides *direct* (and not inferred) observations of fluid properties: sample chambers transport actual liquid or gas samples to the surface for analysis, while properly interpreted pressure transient measurements yield mobility, the ratio of permeability to viscosity, and for multiprobe tools, the anisotropy ratio k_h/k_v – and, of course, there's compressibility and pore pressure.

Despite the importance of formation testers, noting that oil service companies derive significant percentages of their revenue from sampling and real-time pressure transient analysis operations, such tools command relatively low visibility at annual conferences and trade shows – the bulk of existing math modeling papers and patents, in fact, were published in prior decades and assumed some expertise on the part of the reader. Those new to the industry are taught logging basics. For instance, they readily identify resistivity tools as instruments with coils wrapped around drill collars; or, sonic instruments as tools with perforated slots in the metal body; or, gamma ray logging tools, as devices with trademark photo-multipliers and detectors.

But what does a "formation tester" look like? Are there multiple engineering concepts? What are their relative advantages and limitations? How do recent designs differ from earlier ones and how can these be improved? And what exactly underlies advanced tool design, that is, what analysis models are used to develop integrated mechanical and interpretation systems that ensure accurate measurements and predictions in the field? This book addresses these questions, and for completeness, starts with an initial review of prior industry work and also methodologies developed by the authors. The narrative supporting the initial portion of the text is mainly visual, an approach that conveys the greatest volume of information in the least amount of space, while for the latter, beginning with Chapter 7, we focus on three-dimensional quantitative models, computational details and very rigorous validations.

What started as a standalone review on "ideal source models," our scope of work during the early 2000s, has evolved into a companion volume due to Qin et al. (2021) which complements the multiprobe methods of the present book. Like the 3D methods above, source approaches are now routinely used in day-to-day analysis. Importantly, our expositions are deliberately readable – our analysis methods are explained in "plain English" terms with sufficient references to basic math and related prior art – with more than enough detail that motivated students should be able to produce equivalent software prototypes with minor effort. The authors hope that our two latest volumes will provide comprehensive, state-of-the-art reviews for students as well as professionals – and, in fact, a needed resource offering the latest analysis and interpretation techniques, so that formation testing methods become a ubiquitous part of petroleum engineering activities typical of well logging, drilling or reservoir simulation.

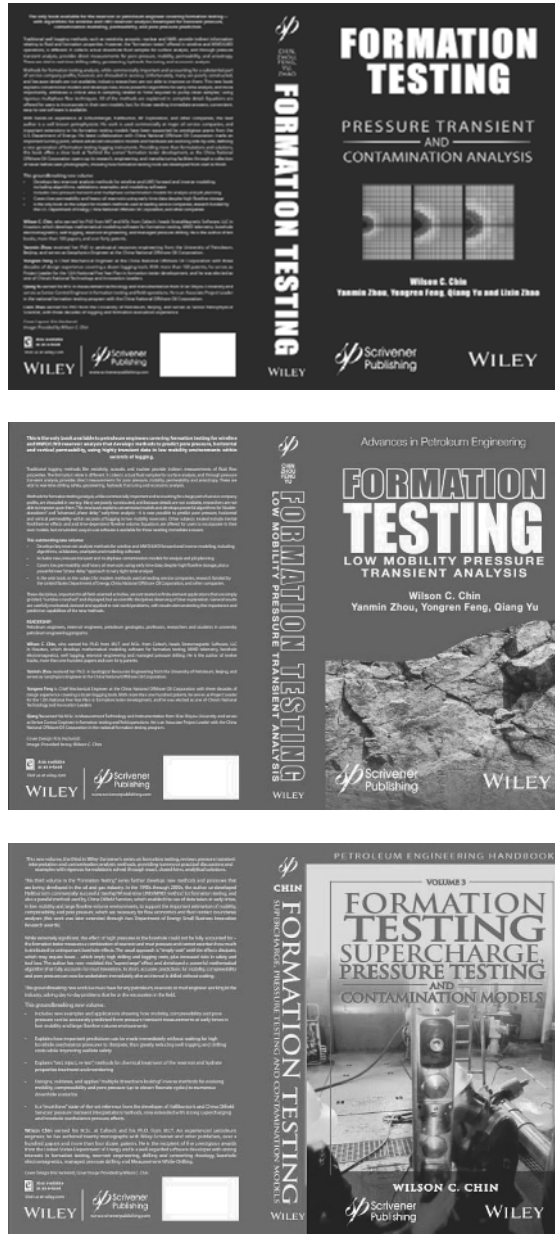

Figure 1.1. Formation testing research monographs, Chin and COSL authors, Scrivener Publishing, 2014, 2015 and 2019.

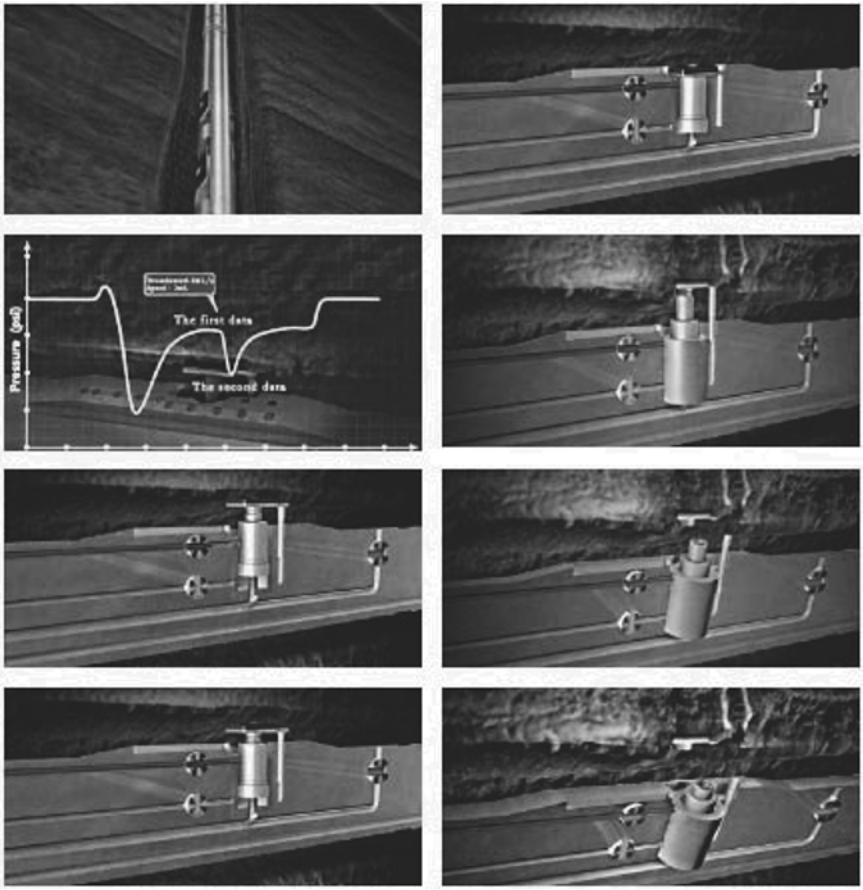

Figure 1.2. Drawdown-buildup pressure responses with dynamic pumping action and flowline.

Remarks. The formation tester is a well logging instrument with nozzles, which when pressed against the borehole sandface, extracts in-situ reservoir fluids for surface analysis. By-products of this process are pressure transients that can be "interrogated" using advanced math models for properties like mobility, anisotropy, compressibility and pore pressure. Testers may be "single" or "multiple probe," positioned axially and/or azimuthally along the tool body. Active probes may withdraw or inject fluids, while passive "observation probes" measure pressures. An example showing two drawdown-buildup curves is given above. Despite the simplicity, sophisticated math models are required for interpretation.

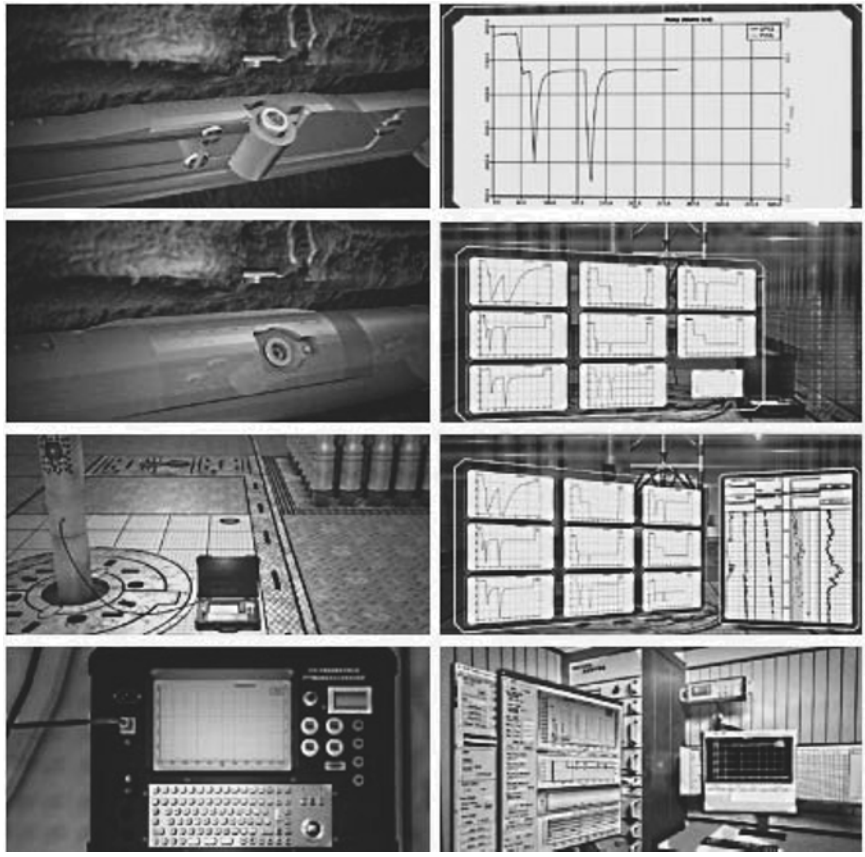

Figure 1.3. Downhole, surface and logging truck operations.

Remarks. Transient pressure responses are collected along the length of the well and predictions for pore pressure and mobility are presented to the petrophysicist as functions of depth. Depending on the data processing requirements of the host math model, real-time calculations can be performed within the tool, at the surface in the logging truck, or when these options are not possible, at the home office where more computing resources are available (data are transmitted for off-site calculation and received as well logs). A logging truck such as that shown will support a wide variety of formation testing software apps, for example, as described in Qin et al. (2021) for "source models" and the present book for triple probe forward and inverse applications.

1.2 Conventional Formation Testing Concepts.

Formation testing design concepts are rich and varied. A pumping probe, operating as a "sink" or a "source," also tracks pressure transient responses. Other pressure probes may reside along the tool body, displaced axially, azimuthally or both, which may actively pump or function as passive observers. While the primary formation tester function is fluid sampling, in which in-situ reservoir fluids are collected and transported to the surface for analysis, pressure measurements represent critical byproducts that are important to formation evaluation. Examples of testers offered by different manufacturers for wireline and MWD applications are given in Figures 1.4 – 1.7.

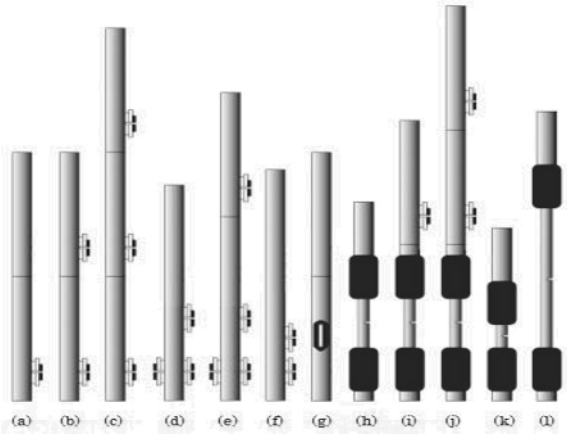

Figure 1.4. Conventional formation tester tool strings.

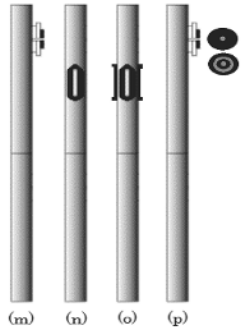

Figure 1.5. Formation testers, additional developments.

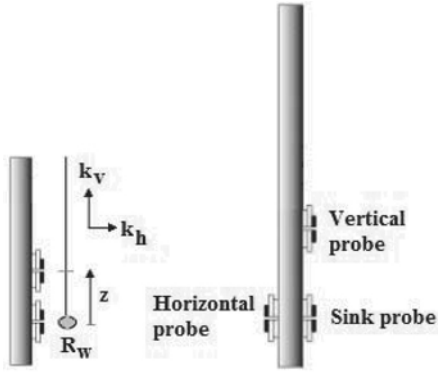

Figure 1.6. Conventional dual and triple probe testers.

Figure 1.7. Dual probe tester with dual packer.

1.3 A New Triple Probe Tool – Design Concepts and Well Logging Advantages.

A well known industry "triple probe" tool is sketched in Figure 1.8. A "sink probe," shown at the top right, withdraws fluid from the formation and initiates a pressure drawdown. The pressure drop is communicated to a "horizontal probe" that is displaced 180° circumferentially about the tool – that is, both sink and horizontal probe lie in the same plane normal to the tool axis. A third "vertical probe" is often found on the tool body at the same azimuth and displaced axially, say about thirty inches away. This conventional triple probe tool is different from the COSL triple probe tool shown in Figure 1.9. The COSL tool consists of three probes set in the same normal plane, each displaced 120° from the others – additionally, one or more axial probes may be installed along the tool string. These are discussed later in this volume, drawing on our 2014, 2015 and 2019 book publications, which have already addressed forward and inverse modeling algorithms for axial probes. The new triple tool hosts several advantages. First, the design offers redundancy and provides an important margin of safety in the event of downhole mechanical failure. Second, if all three probes are

identical, the ability to see at different angles allows the tester to detect heterogeneities that may possibly remain hidden with single probe tools. Third, it is possible to measure dip angle, if distinct thin layers exist. Fourth, equipping the tester with different sized probes, for example, with small, medium and long slotted nozzles, enhances the tool's ability to log formations where little is known about the formation. This is a crucial advantage in exploration applications.

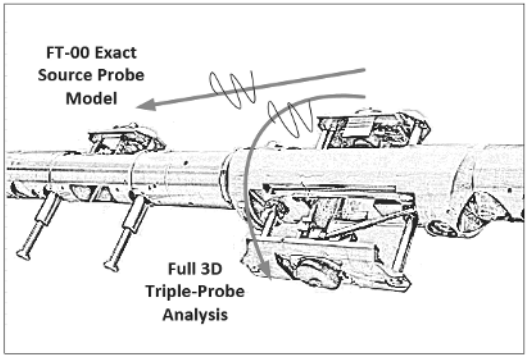

Figure 1.8. Conventional "triple probe" tester with analysis methods.

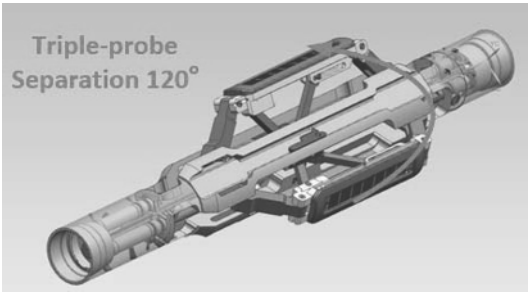

Figure 1.9. COSL "triple probe" arrangement with possibly different nozzle pads – additional axially displaced probes are supported.

Other advantages are apparent. In low permeability formations, commonly used fluid withdrawal rates may result in large drawdowns and undesirable release of damaging dissolved gas. One might, for instance, have two nozzles inject fluids into the formation in order to increase background pressures, with the third performing normal drawdowns while operating above the bubble point.

In this book we address pressure transient logging issues. Several obvious questions arise with regard to the two state-of-the-art testers above. For example, "How do observation probe signals compare in tight formations for the azimuthal designs in Figures 1.8 and Figure 1.9, given the large differences in angular location?" Or, "How significant is the 'vertical probe' in Figure 1.8?" "What is their relative performance?" We will address these questions before embarking on the main objective of this volume – the development of a comprehensive math model for *modern* triple probe formation testers, considering independently operable nozzles, non-negligible flowline volume, general supercharge pressures in overbalanced drilling and "undercharge" in underbalanced applications, actual borehole size and shape, and so on. In short, we will focus on two equally important field objectives. "How can we enhance the pressure transient interpretation process?" "Can we design a model that also serves job planning objectives as well as mechanical design?"

1.3.1 Azimuthal flow signal strength (circumferential probes).

Several of the results in this azimuthal analysis are taken from Example 1 in Chapter 8, which provides greater detail. Our results are based on the algorithm developed and validated in Chapters 7 and 8, a model which addresses the key design objectives of the above paragraph. The user interface in Figure 1.10a was designed to host numerous capabilities conveniently, with a minimal amount of training and expertise required on the part of the user. The left side of the input screen displays the usual parameters needed to define a transient simulation, the fluid and rock inputs being porosity, (liquid) viscosity, compressibility, anisotropic permeability and pore pressure. The value of pore pressure itself is not significant dynamically. That is, whether this hydrostatic value is 20,000 psi or 1,234 psi, the final drawdown and transient evolution will remain unaffected; such numbers being entered for logging convenience only. In many of our examples, we simply enter "0," so that the pressure drop response is easily read from graphs and tabulations and interpreted as the net pressure drawdown (or buildup). Circular cylindrical mesh details and nozzle calibration constants, or "geometric factors," are described in editable files not shown.

For our evaluation run, we assume the fluid, rock and tool inputs specified on the left side of the screen. The cross-section of the plane hosting the triple probe tool is always discretized using circular cylindrical coordinates. Circumferential grids are each 30^o wide, so

twelve are required to represent a complete circle. In our convention, "1" starts at the very bottom, progressing to "3," "7" and "11" going in the counter-clockwise direction. A last nodal position "13" is coincident with "1" and is not displayed – it is simply a grid definition requirement necessary in the solution process. COSL's triple probes are located at "3," "7" and "11" – these nozzles operate independently, may support positive, negative or zero flow rates, with different start and end times, and use any combination of geometric pad designs. Our model is restricted to vertical wells in transversely isotropic media. To facilitate comparisons with two-probe designs such as that in Figure 1.8, we designate "7" as the "sink" and "1" as the passive "horizontal probe." Again, "3," "7" and "11" possess identical pumping and pressure measurement capabilities, but "1" is strictly a passive observation probe which does not pump. At the center of Figure 1.10a is our flow rate menu. For each of the three pumping probes, we may enter a flow rate with custom start and end times (more complicated schedules are also supported). The present calculation assumes that "3" and "11" do not pump, and that "7" pumps with a volume flow rate of 1 cc/s, which starts at t = 0 and ends at t = 99 sec, the maximum time value supported by this interface. Despite its simplicity, it is clear how interacting drawdown and drawdown-buildup processes can be created (flow rates may be positive, negative or zero) which mimic complex field procedures.

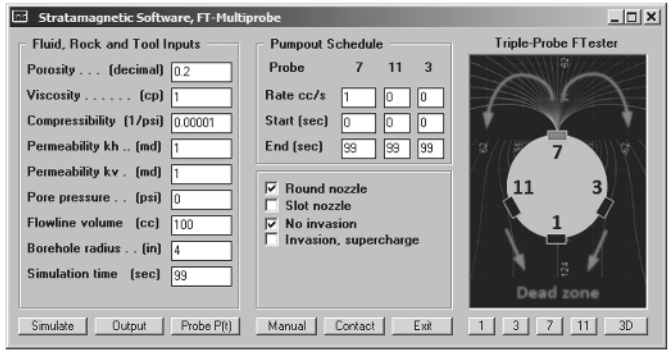

Figure 1.10a. Parameter input screen for interactive calculations.

The central portion of the menu allows the user to select "round" versus "slot" nozzles, and also, "no invasion" versus "invasion, supercharge." Finite difference grid details associated with these options are wired internally and can be changed by using a separate routine.

Clicking "Simulate" launches the numerical time integration and solutions typically appear within seconds on Intel i5 Windows machines.

The line graphs in Figures 1.10b, 1.10c and 1.10d appear automatically on run completion. The first gives the sink probe response at 0^o and it is seen how pressures equilibrate very rapidly at the source, requiring about 15 – 30 sec. The pressure drop is significant, at about 3,500 psi. The calculations are seen to be numerically stable. The results at observation Probe 3 (which are identical with that of Probe 11) are quite different. The pressure drop is much less, about 19 psi, and pressure diffusion implies that steady state requires longer times to achieve. The pressure drop at observation Probe 11 is even smaller, at about 13 psi, and the time needed to equilibrate is likewise slow. Figure 1.10e provides a detailed tabulation of pressures in the circular annular computational domain that wraps about the tool. The indexes K = 1, 2, 3 . . . 13 indicate angular positions. The first row of numbers provides pressure drops along the borehole interface. For example, the "-3,456" beneath the <7> indicates that the pressure drop is 3,456 psi at Probe 7. This decreases to 702 psi and 218 psi going down the column, that is, as radius increases away from the tool at the two subsequent grid blocks. Consider the pressures at adjacent azimuthal nodes "6" and "8." The "207s" at the left and right of "7" properly reflect the left-right symmetry expected on physical grounds. On the other hand, the unchanging "207" pressures going from one row to the next (that is, with radial position increasing from the borehole interface) shows that no-flow conditions are properly enforced (when formation invasion or outflux occur, the pressure drops at the sandface will not be zero). Figure 1.10e also displays the time value and the location of the z plane described by the tabulations. The numerical values shown therefore contain a wealth of information related to the dynamics of the problem and the quality of the solution. They are "must reading" in any interpretation scenario. For the present assumed inputs, the mobilities are low, but not particularly low. The calculations show that the pressure signal at the 120^o location is about 19 psi, while that at the standard 180^o observation location is a much smaller 13 psi. Both are much less than the source probe pressure drop. In tighter formations, the signal advantage offered by the 120^o location over the 180^o location may be significant, since the latter may not fall within the measurement range of the transducer. We now turn to our second question, "What are the implications of separation distance for the axially displaced probes in Figure 1.8?"

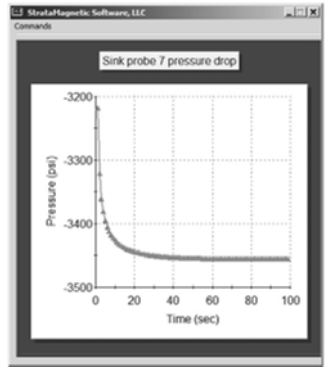

Figure 1.10b. Sink (pumping) Probe 7 pressure response at 0°.

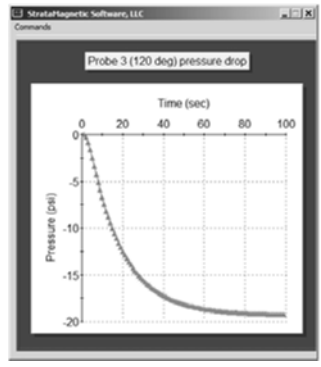

Figure 1.10c. Observation Probe 3 (or 11) pressure response at 120° (note, pressure drop relative to source value is 0.0055).

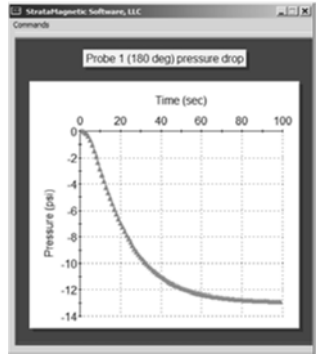

Figure 1.10d. Observation Probe 1 pressure response at 180° (note, pressure drop relative to source value is 0.0038).

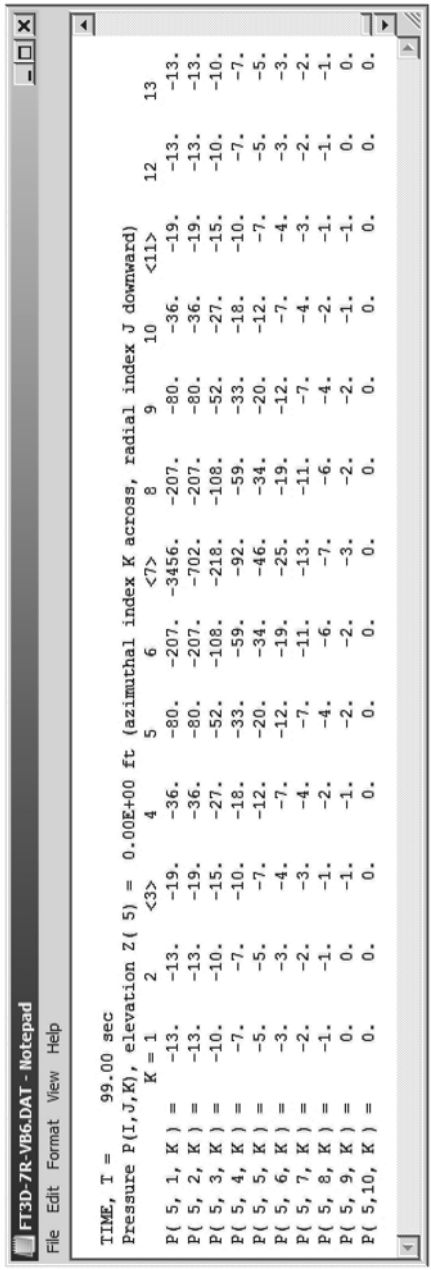

FT3D-7R-VB6.DAT - Notepad

File Edit Format View Help

```
TIME, T =     99.00 sec
Pressure P(I,J,K), elevation Z( 5) =  0.00E+00 ft (azimuthal index K across, radial index J downward)
                K = 1      2      <3>      4      5      6      <7>      8      9     10     <11>     12     13
P( 5, 1, K ) =   -13.   -13.   -19.   -36.   -80.  -207.  -3456.  -207.   -80.   -36.   -19.   -13.   -13.
P( 5, 2, K ) =   -13.   -13.   -19.   -36.   -80.  -207.   -702.  -207.   -80.   -36.   -19.   -13.   -13.
P( 5, 3, K ) =   -10.   -10.   -15.   -27.   -52.  -108.   -218.  -108.   -52.   -27.   -15.   -10.   -10.
P( 5, 4, K ) =    -7.    -7.   -10.   -18.   -33.   -59.    -92.   -59.   -33.   -18.   -10.    -7.    -7.
P( 5, 5, K ) =    -5.    -5.    -7.   -12.   -20.   -34.    -46.   -34.   -20.   -12.    -7.    -5.    -5.
P( 5, 6, K ) =    -3.    -3.    -4.    -7.   -12.   -19.    -25.   -19.   -12.    -7.    -4.    -3.    -3.
P( 5, 7, K ) =    -2.    -2.    -3.    -4.    -7.   -11.    -13.   -11.    -7.    -4.    -3.    -2.    -2.
P( 5, 8, K ) =    -1.    -1.    -1.    -2.    -4.    -6.     -7.    -6.    -4.    -2.    -1.    -1.    -1.
P( 5, 9, K ) =     0.     0.    -1.    -1.    -2.    -2.     -3.    -2.    -2.    -1.    -1.     0.     0.
P( 5,10, K ) =     0.     0.     0.     0.     0.     0.      0.     0.     0.     0.     0.     0.     0.
```

Figure 1.10e. Sink elevation pressure at 99 sec, azimuthal θ_k vs radial r_j.

1.3.2 Axial signal strength (centerline oriented dual probes).

Axially displaced probes can be studied by Model FT-00, developed in Chin et al. (2014), following an exact, closed form, analytical solution assuming a spherical or ellipsoidal source. The user interface for FT-00 is shown in Figure 1.11a. Because the circular model in Section 1.3.1, allowing for full borehole simulation, and the present axial one, are completely different, we need to calibrate FT-00 so that both yield similar sink probe responses for the same input fluid, formation and tool parameters.

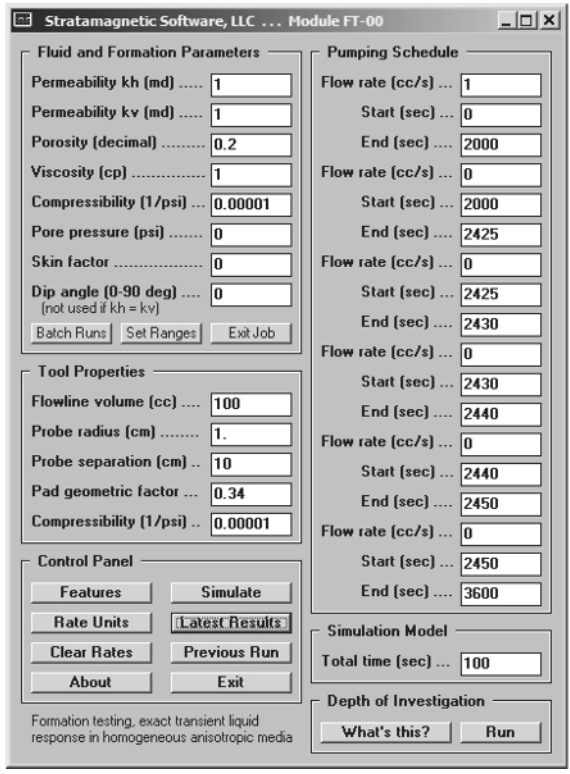

Figure 1.11a. Exact FT-00 source model analysis.

Figures 1.10a and 1.11a show the same input parameters. FT-00 provides for a "geometric factor" calibration input that allows an adhoc adjustment to calculated pressure responses, and is often used as a history matching parameter. In the present case, the choice 0.34 leads to

a source probe pressure response that is almost identical to that of the prior analysis. That is, the source responses in Figures 1.10b and 1.11b are very similar, both yielding about a 3,400 psi pressure drop and about a 20 sec time to steady state. Figure 1.11c provides a detailed tabulation of results for the source probe response.

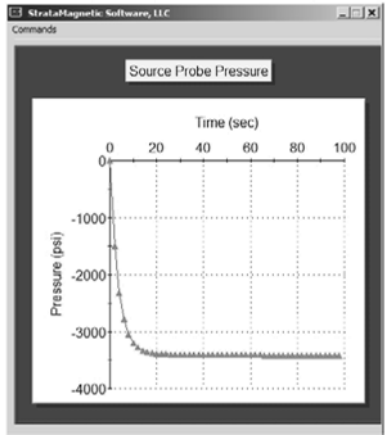

Figure 1.11b. Source probe pressure response.

BASIC.TXT - Notepad

File Edit Format View Help

```
PUMPING SCHEDULE AND SIMULATION PARAMETERS

Total simulation time ..... (sec):   0.1000E+03

DEFINITIONS
Time ... Elapsed time (sec)
Rate ... Drawdown flow rate (cc/s)
Ps* .... Source pressure with hydrostatic (psi)
Pr* .... Observation pressure with hydrostatic (psi)
Ps** ... Source pressure, no hydrostatic (psi)
Pr** ... Observation pressure, no hydrostatic (psi)

         NOTE: Ps* or Pr* < 0 means volume flow
         rate cannot be achieved in practice

 Time (s)  Rate (cc/s)    Ps* (psi)     Pr* (psi)    Ps**(psi)    Pr**(psi)    Pr**/Ps**
0.000E+00  0.10000E+01  0.00000E+00  0.00000E+00  0.00000E+00  0.00000E+00  ----------
0.200E+01  0.10000E+01 -0.14929E+04 -0.76001E+02 -0.14929E+04 -0.76001E+02  0.50908E-01
0.400E+01  0.10000E+01 -0.23203E+04 -0.10644E+03 -0.23203E+04 -0.10644E+03  0.45872E-01
0.600E+01  0.10000E+01 -0.27839E+04 -0.11769E+03 -0.27839E+04 -0.11769E+03  0.42276E-01
0.800E+01  0.10000E+01 -0.30456E+04 -0.12177E+03 -0.30456E+04 -0.12177E+03  0.39982E-01
0.100E+02  0.10000E+01 -0.31944E+04 -0.12293E+03 -0.31944E+04 -0.12293E+03  0.38481E-01
.
.
.
0.200E+02  0.10000E+01 -0.33867E+04 -0.12083E+03 -0.33867E+04 -0.12083E+03  0.35676E-01
0.300E+02  0.10000E+01 -0.34050E+04 -0.11930E+03 -0.34050E+04 -0.11930E+03  0.35037E-01
0.400E+02  0.10000E+01 -0.34097E+04 -0.11861E+03 -0.34097E+04 -0.11861E+03  0.34787E-01
0.500E+02  0.10000E+01 -0.34123E+04 -0.11824E+03 -0.34123E+04 -0.11824E+03  0.34652E-01
0.600E+02  0.10000E+01 -0.34140E+04 -0.11801E+03 -0.34140E+04 -0.11801E+03  0.34566E-01
0.700E+02  0.10000E+01 -0.34153E+04 -0.11784E+03 -0.34153E+04 -0.11784E+03  0.34505E-01
0.800E+02  0.10000E+01 -0.34163E+04 -0.11772E+03 -0.34163E+04 -0.11772E+03  0.34460E-01
0.900E+02  0.10000E+01 -0.34171E+04 -0.11763E+03 -0.34171E+04 -0.11763E+03  0.34424E-01
```

Figure 1.11c. Tabulated pressures versus time.

The tabulated results in Figure 1.11c closely correspond to those obtained from the azimuthal flow solver, that is -3,417 psi using FT-00 and – 3,456 psi from the full three-dimensional code. This agreement at the sink (or, source) point provides the needed calibration process, so vertical (and other axial) probe results can be meaningfully compared to azimuthal ones like the horizontal probe. Once the calibration is completed, we click the Depth of Investigation "Run" button at the bottom right of Figure 1.11a. This action leads to the screen in Figure 1.11d. Its driving algorithm is identical to that of FT-00. However, its flow rate schedule is simpler, allowing a constant rate input only. Pressure versus time responses are automatically created every ten centimeters from the source probe. These are replicated in Figures 1.11e – 1.11k, that is, until 80 cm or approximately 31 inches. The complete sequence of calculations requires about 1-2 minutes of "desk time."

The calculated results show that at 80 cm, or about 31 in, the pressure drop has decreased from about 3,400 psi at the source to 7 psi, or about three orders of magnitude. However, this signal in practice is useless because pressure diffusion would have widened the disturbance so much that it would be difficult to discern. For this reason, COSL and other manufacturers have chosen axial spacings of about 6 – 8 in for their basic conventional dual probe tools. Figure 1.11f shows a relatively rapid equilibration to steady state and a sizable signal of about 55 psi. It is also interesting to compare the 80 cm "vertical probe" signal to that of the 180^{o} "horizontal probe." Again, at 80 cm, we have about 7.5 psi from Figure 1.11k, whereas we have 13 psi from Figure 1.10d. This suggests that the observation probe measurement is superior to the 80 cm result. The results of this section represent only one specific calculation and one should not infer more general conclusions. Numerous other simulations demonstrating the features of the new triple probe tool are given in Chapters 8 and 9. Further comments on the 180^{o} tool are given in Section 1.3.3 next.

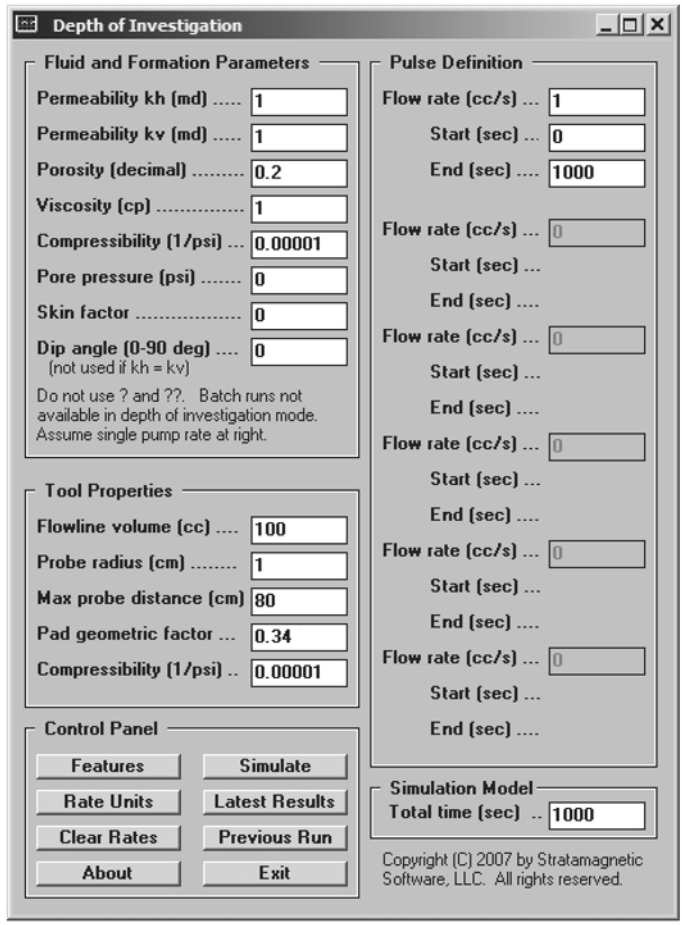

Figure 1.11d. Depth of investigation calculator.

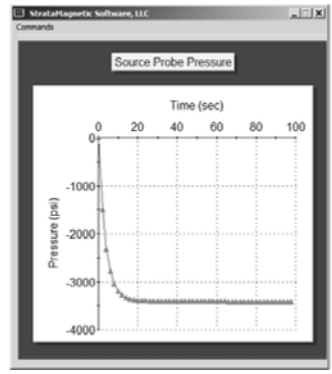

Figure 1.11e. Source probe response, very rapid equilibrium.

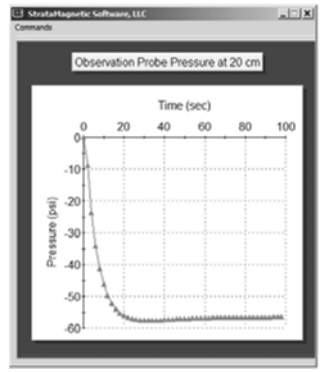

Figure 1.11f. Pressure response at 20 cm (about 8 inches).

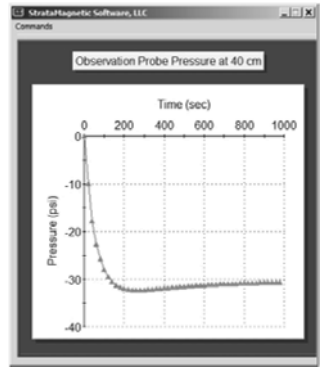

Figure 1.11g. Pressure response at 40 cm.

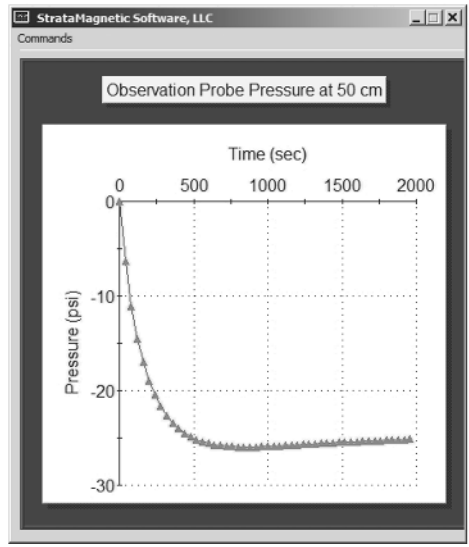

Figure 1.11h. Pressure response at 50 cm.

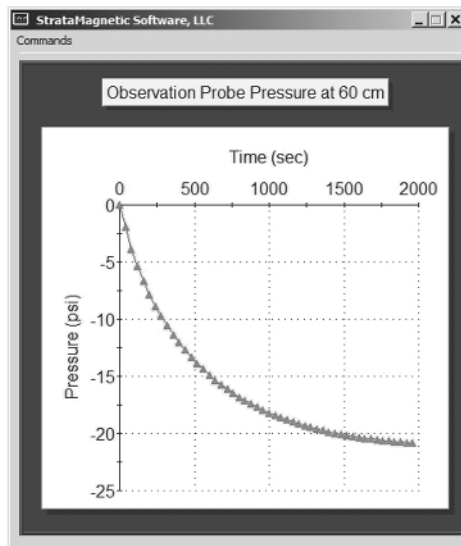

Figure 1.11i. Pressure response at 60 cm.

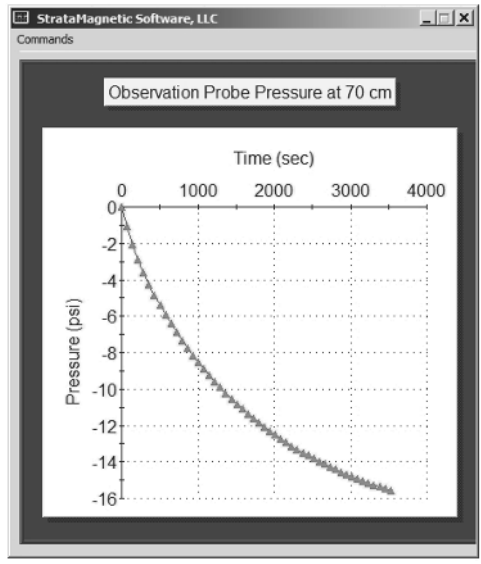

Figure 1.11j. Unequilibrated pressure response at 70 cm.

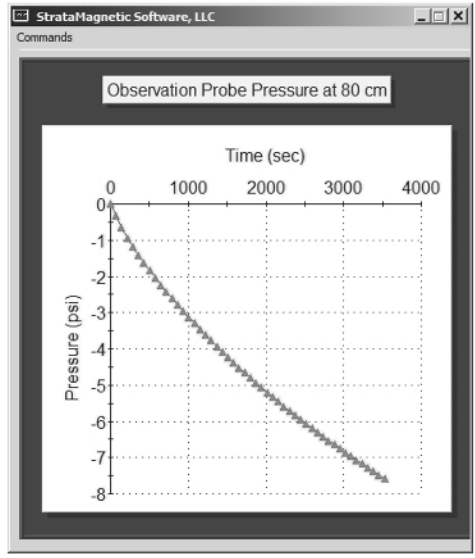

Figure 1.11k. Unequilibrated pressure at 80 cm (about 31 inches).

1.3.3 Hardware and software considerations.

In this section, we address other issues of concern that motivated the COSL triple probe design in Figure 1.9. This decision in turn prompted the development of advanced fluid simulation models that would support mechanical optimization and formation evaluation interpretation efforts. This topics are briefly summarized below.

Probe architecture selection. During the initial development of Halliburton's "Reservoir Description Tool" or RDT^{TM} in the 1990s, the last author and co-researchers had produced azimuthal and axial pressure results similar to those in Section 1.3.2 but using a commercial finite difference simulator. As a result, the company chose a different development path, opting for a "dual probe" design with axially separated transducers of about seven inches – thirty inch separations or probes displaced 180^{o} diametrically were not considered. Halliburton's tool was supported by real-time downhole interpretation software, known commercially by GeoTap^{TM} – this was developed by the last author, with the model giving effective permeability, compressibility and pore pressure. The combined system was tested and calibrated experimentally, with field results proving to be very useful.

Recently, a well known industry expert affiliated with a large Middle East company offered his opinion regarding the original triple probe tool. The "module was never very popular when introduced in the 1990s and was never widely used. However, it was continually promoted over the years. If you look closely at most published examples, the pressure changes at the two observation probes are very small, and as you said, have virtually no transient response (one probe at 180 deg and the other about two feet axially from the sink). Currently most vertical interference testing is performed using straddle packers with vertical observation probes." In fact, "a newer three-dimensional tool, basically four oval probes arranged around an inflatable packer, is being promoted. The larger probes and straddle packers enable drawdowns with much larger fluid volumes, which are necessary to measure a response from the vertical observation probes that are 3 to 6 ft away."

China Oilfield Services Limited, while it does manufacture dual probe formation testers of the Halliburton type as illustrated in Figure 1.12, is focusing its higher end tools towards "triple probe" designs as shown in Figure 1.9 and 1.13. Again, 120^{o} angle separations provide stronger signals than would be possible with 180^{o} designs, and versatility is enhanced by allowing each probe to operate independently and transiently – as noted, the triple probe arrangement in Figure 1.13 will be augmented by one or more axially displaced probes. A wide range of job planning and "inverse" applications is presented in this volume, made possible by the fully three-dimensional and rapid transient simulator developed here. We emphasize that *this* book deals with the new azimuthal triple probe system while the companion and complementary volume of Qin et al. (2021) addresses source models that are also important to different axial displacement aspects of the present design.

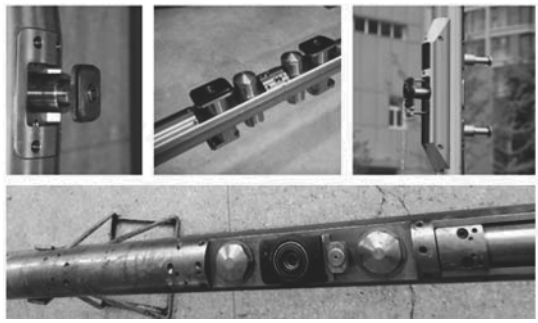

Figure 1.12. Early COSL single and dual probe formation testers (details in 2014 and 2015 books).

Figure 1.13. New COSL azimuthal triple probe formation tester.

Simulation considerations. A significant effort was made by the authors to understand and replicate published results related to the Schlumberger MDT™ tool. While excellent reviews have been offered over the years in *Oilfield Review*, these lacked the details developers required to offer enhanced products – one important objective, of course, being able to create interpretation platforms that provide greater value. While proprietary software may well exist, the authors were (and are not) aware of any strong capabilities openly available in the public domain. After an extensive search, we turned to two papers which are studied in detail in Chapter 5 and 6, namely,

- "Multilayer Reservoir Testing with Multiprobe Wireline Formation Tester," by F.J. Kuchuk, T.S. Ramakrishnan, C. Ayan, M. Akbar and Y. Mahmoud (Schlumberger), and N. Young and S. Al-Matroushi (ADCO – Abu Dhabi, U.A.E.), SPE Paper 36176, presented at the Seventh Abu Dhabi International Petroleum Exhibition and Conference, Abu Dhabi, U.A.E., 13-16 October 1996, and
- "Lessons Learned from Wireline Formation Testing with Single and Multiple Probes," by H.J. Su (Chevron Overseas Petroleum Technology Company), K.G. Al-Anezi and S.P. Sinha (Kuwait Oil Company), and A.G. Ceyhan (Schlumberger Kuwait), SPE Paper 68143, presented at the 2001 Middle East Oil Show held in Bahrain, 17-20 March 2001.

Commercial formation testing software is also noticeably absent. While generic finite element simulations, e.g., Ansys™, Fluent™, Solidworks™ and others, are available, they require specialized skills and detailed setup and run times. Kappa Engineering's KAPPA module, known as Azurite, can analyze or simulate all MDT configurations including its triple probe module. Azurite can also analyze/simulate an oval elongated probes, straddle packers and Saturn probes with vertical observation probes (this uses an analytical model developed by Leif Larsen and a numerical simulator to a limited degree). However, in the two papers noted above, and in available simulation brochures, the authors are not aware of algorithms that apply to special applications that are the subject of our focus. These include (1) general modeling of independently operable probes, with different pumping schedules and nozzles, (2) incorporation of supercharge and borehole invasion effects, and (3) extremely rapid "big data" objectives that support creation of massive data sets for real-time inverse applications.

1.3.4 Closing remarks.

This volume, again, focuses on the capabilities behind the new generation of formation testing tools conceptualized by Figures 1.9 and 1.13, and the development of rapid and stable numerical transient and steady flow simulators which support optimized mechanical design, job planning and advanced interpretation. A companion book of Qin et al. (2021) addresses recent "ideal source" developments for forward and inverse problems in formation testing, including supercharge effects and permeability prediction using discrete pairs of "pressure and time" data in the presence of variable pump rate schedules.

1.4 References.

- Chin, W.C., *Formation Testing: Supercharge, Pressure Testing and Contamination*, John Wiley & Sons, Hoboken, New Jersey, 2019.
- Chin, W.C., Zhou, Y., Feng, Y. and Yu, Q., *Formation Testing: Low Mobility Pressure Transient Analysis*, John Wiley & Sons, Hoboken, New Jersey, 2015.
- Chin, W.C., Zhou, Y., Feng, Y., Yu, Q. and Zhao, L., *Formation Testing: Pressure Transient and Contamination Analysis*, John Wiley & Sons, Hoboken, New Jersey, 2014.
- Kuchuk, F.J., Ramakrishnan, T.S., Ayan, C., Akbar, M., Mahmoud, Y., Young, N. and S. Al-Matroushi "Multilayer Reservoir Testing with Multiprobe Wireline Formation Tester,"SPE Paper 36176, presented at the Seventh Abu Dhabi International Petroleum Exhibition and Conference, Abu Dhabi, U.A.E., 13-16 October 1996.
- Su, H.J., Al-Anezi, K.G., Sinha, S.P. and Ceyhan, A.G.,, "Lessons Learned from Wireline Formation Testing with Single and Multiple Probes,"SPE Paper 68143, presented at the 2001 Middle East Oil Show held in Bahrain, 17-20 March 2001.